Inverse scattering algorithm for reconstructing lossy fiber Bragg gratings

Amir Rosenthal and Moshe Horowitz

Department of Electrical Engineering, Technion–Israel Institute of Technology, Haifa 32000 Israel

We demonstrate an inverse scattering algorithm for reconstructing the structure of lossy fiber Bragg gratings. The algorithm enables us to extract the profiles of the refractive index and the loss coefficient along the grating from the grating transmission spectrum and from the reflection spectra, measured from both sides of the grating. Such an algorithm can be used to develop novel distributed evanescent-wave fiber Bragg sensors that measure the change in both the refractive index and the attenuation coefficient of the medium surrounding the grating. The algorithm can also be used to analyze and to design fiber Bragg gratings written in fiber amplifiers. A novel method to overcome instability problems in extracting the parameters of the lossy grating is introduced. The new method also makes it possible to reduce the spectral resolution needed to accurately extract the grating parameters. © 2004 Optical Society of America

OCIS codes: 050.2770, 060.2370.

1. INTRODUCTION

In recent years, there has been intensive work in the field of fiber optic sensors. Fiber sensors are low cost, are reliable, and are not affected by electromagnetic interference.[1] Fiber Bragg gratings can be used as distributed sensors for measuring the profile of strain or temperature along the grating with a resolution on the order of tens of micrometers.[2–4] The interrogation of such sensors is based on extracting the refractive index of the grating from the complex reflection spectrum by using the Fourier or the Gabor transform.[2] Evanescent-field fiber sensors are used to measure the absorption or the refractive index of the medium surrounding the fiber. The absorption of the medium surrounding the sensor can be found by measuring the total loss in the sensor.[5–11] The change in the refractive index of the medium surrounding the fiber, averaged along the whole sensor length, can be found by using an interferometer or a grating.[12,13] In a previous paper we showed that an evanescent-wave fiber Bragg grating can be used as a distributed sensor with a resolution on the order of tens of micrometers.[14] The impulse response of the evanescent-wave fiber Bragg grating was measured by using low-coherence spectral interferometry performed in the frequency domain.[14,15] The change in the refractive index of the medium surrounding the fiber was extracted by using the Fourier transform. However, in an evanescent-field sensor based on a fiber Bragg grating, the absorption coefficient as well as the effective refractive index changes along the grating. Therefore the measurement of the loss profile in an evanescent-field fiber Bragg sensor can add important information about the medium surrounding the fiber. Extracting the spatial distribution of both the loss and the effective refractive index of the grating may make it possible to develop novel evanescent-field sensors for interrogating highly absorbing media such as biological tissues. The measurement of the absorption profile of the gratings

may also help to detect defects in the grating and to improve the writing process.

Inverse scattering algorithms were used in previous work to extract the refractive-index profile of fiber Bragg gratings when the loss of the grating was neglected.[16–18] Inverse scattering algorithms for extracting the profile of discrete layered lossy structures have been used to study electromagnetic transmission lines.[19,20] In this paper we demonstrate an inverse scattering algorithm that enables us to reconstruct the structure of fiber Bragg gratings with loss. The algorithm permits determination of both the effective refractive index and the absorption profile along the grating. The algorithm is based on a layer-peeling technique described in Refs. 19 and 20. A new method was added to the algorithm to overcome instabilities that may arise when a grating with high reflectivity and/or high loss is analyzed. Such an instability can occur during analysis of fiber Bragg gratings. The new method for solving the instability problem also permits reduction of the spectral resolution needed to present the grating spectra. Therefore the spectral resolution needed in the algorithm described in this paper is smaller than the resolution required in previously published algorithms for analyzing highly reflecting lossless fiber Bragg gratings. The derivation of the algorithm in this paper does not require definition of a noncausal signal as in Ref. 19. Unlike in Ref. 20, we use a continuous formulation for the direct scattering problem. We also use a complex coupling coefficient for analyzing the grating rather than the real coupling coefficient used in Refs. 19 and 20. We note that the inverse scattering algorithm for interrogating lossy fiber Bragg gratings described in this paper may also be used to interrogate fiber gratings written in amplifying media, such as Erbium-doped fiber amplifiers. Therefore the algorithm may also be important for interrogating active sensors and distributed fiber Bragg lasers.[21]

2. MATHEMATICAL MODEL

In this section we give the mathematical model needed to solve the inverse scattering problem for lossy fiber Bragg gratings written in single-mode fibers. Our analysis in this section is based on coupled-mode theory.[22,23] The grating can be modeled as a perturbation to the refractive index along the fiber,

$$n_{\text{eff}}(z) = n_{\text{avg}} + n_0(z) + i\,\eta(z) + n_1(z)\sin\left[\frac{2\pi}{\Lambda}z + \theta(z)\right],$$

$$(1)$$

where n_{avg} is the average refractive index, $n_0(z)$ is the spatially dependent average refractive index, $\eta(z)$ is the spatially dependent average absorption coefficient, $n_1(z)$ is the amplitude of the refractive-index modulation, and Λ is the average grating period. We assume that the functions $n_0(z)$, $\eta(z)$, $n_1(z)$, and $\theta(z)$ are slowly varying with respect to the grating period. We also assume that the refractive index and the absorption of the grating do not depend on the wavelength.

The electrical field is presented as a superposition of the backward- and the forward-propagating fields,

$$E(x, y, z, t) = [a_1(z)\exp(-i\beta z)$$
$$+ a_2(z)\exp(i\beta z)]e(x, y)\exp(-i\omega t),$$
$$(2)$$

where $a_1(z)$ and $a_2(z)$ are the slowly varying amplitudes of the waves propagating in the $-z$ and $+z$ direction, respectively; $e(x, y)$ is the transverse distribution of the field; and $\beta = \omega n_{\text{avg}}/c$ is the wave number, where c is the speed of light in vacuum. Using coupled-mode theory and averaging over the transverse field distribution,[23] we obtain

$$\frac{\mathrm{d}a_1(z)}{\mathrm{d}z} = -ia_1(z)[\sigma(z) + i\alpha(z)] + a_2(z)\kappa(z)$$
$$\times \exp(-i\theta(z) + 2ikz),$$

$$\frac{\mathrm{d}a_2(z)}{\mathrm{d}z} = ia_2(z)[\sigma(z) + i\alpha(z)] + a_1(k)\kappa(z)$$
$$\times \exp(i\theta(z) - 2ikz), \qquad (3)$$

where $k = \beta - \beta_B$ is the wave number detuning with respect to the Bragg design wave number $\beta_B = \pi/\Lambda$ and the coefficients $\sigma(z)$, $\eta(z)$, and $\kappa(z)$ are equal to

$$\sigma(z) = \frac{\omega}{c}\frac{\displaystyle\int n_0(x, y, z)|e(x, y)|^2\mathrm{d}x\,\mathrm{d}y}{\displaystyle\int |e(x, y)|^2\mathrm{d}x\,\mathrm{d}y},$$

$$\alpha(z) = \frac{\omega}{c}\frac{\displaystyle\int \eta(x, y, z)|e(x, y)|^2\mathrm{d}x\,\mathrm{d}y}{\displaystyle\int |e(x, y)|^2\mathrm{d}x\,\mathrm{d}y},$$

$$\kappa(z) = \frac{\omega}{c}\frac{\displaystyle\int n_1(x, y, z)|e(x, y)|^2\mathrm{d}x\,\mathrm{d}y}{\displaystyle\int |e(x, y)|^2\mathrm{d}x\,\mathrm{d}y}. \qquad (4)$$

Using a vectorial notation $V(k, z) = (v_1(k, z), v_2(k, z))^t$, and using the transformation

$$v_1(k, z) = a_1(k, z)$$
$$\times \exp\left[-ikz - \int_0^z \alpha(\zeta)\mathrm{d}\zeta + i\int_0^z \sigma(\zeta)\mathrm{d}\zeta\right],$$

$$v_2(k, z) = a_2(k, z)$$
$$\times \exp\left[+ikz + \int_0^z \alpha(\zeta)\mathrm{d}\zeta - i\int_0^z \sigma(\zeta)\mathrm{d}\zeta\right],$$

$$(5)$$

we obtain

$$\frac{\mathrm{d}V(k, z)}{\mathrm{d}z} = \begin{bmatrix} -ik & q_1(z) \\ q_2(z) & ik \end{bmatrix} V(k, z), \qquad (6)$$

where $z = 0$ denotes the location where the grating structure begins. The coupling coefficients, $q_1(z)$ and $q_2(z)$, are given by

$$q_1(z) = q(z)\exp\left[-2\int_0^z \alpha(\zeta)\mathrm{d}\zeta\right],$$

$$q_2(z) = q^*(z)\exp\left[+2\int_0^z \alpha(\zeta)\mathrm{d}\zeta\right]. \qquad (7)$$

The coupling coefficient $q(z)$ contains information about the refractive-index structure of the grating and is given by

$$q(z) = \kappa(z)\exp\left[-i\theta(z) + 2i\int_0^z \sigma(\zeta)\mathrm{d}\zeta\right]. \qquad (8)$$

We note that Eq. (6) resembles the coupled-mode equations for a lossless grating[18]; However, when the grating is lossy, the coupling coefficients in Eq. (6), $q_1(z)$ and $q_2(z)$, are two independent functions. The difference between the two coupling coefficients is determined by the absorption.

In a lossless grating, the measurement of the complex reflection from one side of the grating is sufficient to reconstruct the grating profile.[24] However, in a lossy grating, the coupling coefficients $q_1(z)$ and $q_2(z)$ are two independent functions, and therefore additional information is needed in order to uniquely determine the grating parameters. Additional information on the grat-

ing structure can be obtained by measuring the complex transmission and reflection functions from both sides of the grating. Measurement of the reflection spectrum from both sides of a grating has been used previously for extracting the profile of highly reflecting fiber Bragg gratings.[25] A similar experimental setup may be used to measure the structure of lossy gratings.

We assume that the grating is written in the region $[0, L]$. To mathematically define the reflection and the transmission functions from both sides of the grating, we introduce four solutions to the coupled-mode equations [Eq. (6)]: $\Phi(k, z)$, $\bar{\Phi}(k, z)$, $\Psi(k, z)$, $\bar{\Psi}(k, z)$, with the following boundary conditions[24]:

$$\Phi(k, z = 0) = \begin{pmatrix} 1 \\ 0 \end{pmatrix}, \qquad \Psi(k, z = L) = \begin{pmatrix} 0 \\ 1 \end{pmatrix},$$

$$\bar{\Phi}(k, z = 0) = \begin{pmatrix} 0 \\ 1 \end{pmatrix}, \qquad \bar{\Psi}(k, z = L) = \begin{pmatrix} 1 \\ 0 \end{pmatrix}. \qquad (9)$$

The Wronskian of two solutions to Eq. (6), $V = (v_1, v_2)^t$ and $U = (u_1, u_2)^t$, is defined as $W(U, V) = u_1 v_2 - u_2 v_1$. Using Eq. (6) we can show that for any two solutions U and V, $\mathrm{d}/\mathrm{d}z[W(U, V)] = 0$. Using this relation and the boundary conditions in Eqs. (9), we obtain that the Wronskian of the solutions $\Phi(k, z)$ and $\bar{\Phi}(k, z)$ is equal to $W(\Phi, \bar{\Phi}) = 1$. Hence the two solutions $\Phi(k, z)$ and $\bar{\Phi}(k, z)$ are independent. Since Eq. (6) is linear, each of its solutions can be expressed as a linear combination of two independent solutions to Eq. (6):

$$\Psi(k, z) = a(k)\bar{\Phi}(k, z) + b(k)\Phi(k, z),$$

$$\bar{\Psi}(k, z) = \bar{a}(k)\Phi(k, z) + \bar{b}(k)\bar{\Phi}(k, z). \qquad (10)$$

A connection between the coefficients $a(k)$, $b(k)$, $\bar{a}(k)$, $\bar{b}(k)$, can be obtained from the Wronskian of the solutions $\Psi(k, z)$ and $\bar{\Psi}(k, z)$. Using the boundary conditions in Eqs. (9), we obtain $W(\Psi, \bar{\Psi}) = -1$. Substituting Eqs. (10) into the Wronskian $W(\Psi, \bar{\Psi})$, we obtain a connection between the coefficients:

$$b(k)\bar{b}(k) - a(k)\bar{a}(k) = -1. \qquad (11)$$

To define the complex transmission and reflection functions of the grating we refer to the solution of Eq. (6), $U(k, z) = (u_1(k, z), u_2(k, z))^t = \Psi(k, z)/a(k)$. The solution $U(k, z)$ satisfies the boundary conditions $u_2(k, z = 0) = 1$ and $u_1(k, z = L) = 0$, and therefore it describes the scattering of a forward-propagating wave that enters at the left side of the grating, $z = 0$. The forward reflection of the grating is defined as the ratio between the backward- and the forward-propagating waves at the grating input end, $z = 0$: $r^f(k) = u_1(k, z = 0)/u_2(k, z = 0) = b(k)/a(k)$. The forward transmission of the grating is defined as the transmission of the forward-propagating wave: $t^f(k) = u_2(k, z = L)/u_2(k, z = 0) = 1/a(k)$. The forward impulse response of the grating is equal to the Fourier transform of the forward reflection, $h^f(\tau) = (1/2\pi)\int_{-\infty}^{\infty} r^f(k) \times \exp(-ik\tau)\mathrm{d}k$. When the grating reflection is low and the Born approximation can be used accurately, the coupling coefficient $q_1(z)$ can be extracted directly from the forward impulse response, $q_1(z) = -2h^f(2z)$, as obtained

in lossless gratings.[18] However, as can be seen in Eqs. (7), the extraction of the coupling coefficient $q_1(z)$, does not make possible separation between the refractive-index amplitude of the grating $|q(z)|$ and the absorption coefficient $\alpha(z)$. Therefore the forward reflection is not sufficient for extracting the grating parameters even in the simple case of weak gratings, when the Born approximation can be used.

The scattering of a backward-propagating wave that enters at the right side of the grating, $z = L$, may also be described by using the coefficients, $a(k)$, $b(k)$, $\bar{a}(k)$, $\bar{b}(k)$. The solution $\Phi(k, z)$ can be written as a linear combination of the functions $\Psi(k, z)$ and $\bar{\Psi}(k, z)$. Using Eqs. (10) and (11), we obtain $\Phi(k, z) = a(k)\bar{\Psi}(k, z) - \bar{b}(k)\Psi(k, z)$. The backward reflection and transmission of the grating are equal to $r^b(k) = -\bar{b}(k)/a(k)$ and $t^b(k) = 1/a(k)$, respectively. Therefore, the backward and the forward transmission functions are equal: $t(k) = t^f(k) = t^b(k)$. The transmission function as well as both the forward and the backward reflection functions are needed to extract the grating parameters in the layer-peeling algorithm, as described in Section 4. Since the forward and the backward reflection functions are defined at different sides of the grating whereas the peeling algorithm, to be described in Section 4, is performed from one side of the grating, we introduce a conjugate scattering system.

We refer to the solution to Eq. (6), $\bar{U}(k, z) = \bar{\Psi}(k, z)/\bar{a}(k)$, that satisfies the boundary conditions: $\bar{u}_1(k, z = 0) = 1$ and $\bar{u}_2(k, z = L) = 0$. We define a function $\tilde{U}(k, z) = (\tilde{u}_1(k, z), \tilde{u}_2(k, z))^t \equiv (\bar{u}_2(-k, z), \bar{u}_1(-k, z))^t$. The function $\tilde{U}(k, z)$ is a solution of the following coupled-mode equations:

$$\frac{\mathrm{d}\tilde{U}(k, z)}{\mathrm{d}z} = \begin{bmatrix} -ik & q_2(z) \\ q_1(z) & ik \end{bmatrix} \tilde{U}(k, z), \qquad (12)$$

with the boundary conditions $\tilde{u}_2(k, z = 0) = 1$ and $\tilde{u}_1(k, z = L) = 0$. We will refer to the scattering system described by Eq. (12) as the conjugate scattering system. The coupled-mode equations, given in Eq. (12), describe the scattering from a grating with coupling coefficients $q_2(z)$ and $q_1(z)$. The difference between the conjugate and the original scattering systems, described in Eq. (6), is the swapping of the coupling coefficients $q_1(z)$ and $q_2(z)$. The physical meaning of the swapping of the coupling coefficients $q_1(z)$ and $q_2(z)$ can be understood from the definition of the coupling coefficients in Eq. (7): The loss coefficient $\alpha(z)$ in the original problem is converted into a gain coefficient $-\alpha(z)$ in the conjugate problem. Therefore, when the original system corresponds to a lossy grating, the conjugate system corresponds to a grating written in an amplifying medium. Similarly to the definitions in the original scattering problem, we define the forward reflection of the conjugate scattering problem by $\tilde{r}^f(k) = \bar{b}(-k)/\bar{a}(-k)$. When the conjugate system is stable, its forward impulse response is given by $\tilde{h}^f(\tau) = (1/2\pi)\int_{-\infty}^{\infty} \tilde{r}^f(k)\exp(-ik\tau)\mathrm{d}k$. Since the conjugate system corresponds to a grating written in an amplifying me-

dium, its solution may become unstable. The stability of the conjugate scattering system is discussed in Section 3.

We note that the forward reflection function of the conjugate system cannot be measured experimentally, since it corresponds to a grating that does not really exist. However, using the connections $\bar{b}(k) = -r^b(k)/t(k)$, $b(k) = r^f(k)/t(k)$, and Eq. (11), we can find the forward reflection of the conjugate system, $\tilde{r}^f(k)$:

$$\tilde{r}^f(k) = -\frac{r^b(-k)}{[t(-k)]^2 - r^f(-k)r^b(-k)}. \qquad (13)$$

We note that the reflection and transmission functions used in Eq. (13) were defined after transforming the fields with Eqs. (5). To connect the reflections and transmission $r^f(k)$, $r^b(k)$, $t^f(k)$ to the measurable reflections and transmission $r_m^f(k)$, $r_m^b(k)$, $t_m^f(k)$, one should use the following transformation:

$$r_m^f(k) \to r^f(k),$$

$$t_m(k)\exp\left[+ikL + \int_0^L \alpha(\zeta)\mathrm{d}\zeta - i\int_0^L \sigma(\zeta)\mathrm{d}\zeta\right] \to t(k),$$

$$r_m^b(k)\exp\left[+2ikL + 2\int_0^L \alpha(\zeta)\mathrm{d}\zeta - 2i\int_0^L \sigma(\zeta)\mathrm{d}\zeta\right]$$
$$\to r^b(k). \qquad (14)$$

Although the backward reflection and the transmission functions change because of the transformation, Eq. (13) remains the same when the measurable reflection and transmission functions $r_m^f(k)$, $r_m^b(k)$, $t_m^f(k)$ are substituted for the transformed functions $r^f(k)$, $r^b(k)$, $t^f(k)$. Therefore the forward reflection functions of the original and the conjugate systems do not change, in spite of the variable transformation in Eqs. (5). Since the transmission function of the grating has a minimal phase, the transmission intensity can be measured and can be used to calculate the transmission phase by the Hilbert transform.[26] A linear phase shift $\exp(ikL)$ should be added to the transmission function, calculated by the Hilbert transform, where L is the grating length. The grating length L can be extracted from the functions $a(k)$ and $b(k)$, as explained in Section 3.

3. STABILITY OF THE CONJUGATE SYSTEM

In this section we introduce a new method for solving the instability problem that may arise in the conjugate scattering system. When the grating in the original problem is lossy, the conjugate system describes a grating written in an amplifying medium. The combined effect of the grating feedback and the amplification may cause the impulse response to become unstable. When the impulse response is unstable, the system behaves as a laser that operates above threshold without the saturation effect that stabilizes a laser operation. In this case, the energy of the impulse response becomes infinite, and the impulse-response function cannot be calculated by performing a Fourier transform on the reflection spectrum.

In this section we show that the instability problem can be solved by extending the solutions given in Eqs. (9) to complex frequencies $\kappa = k + i\eta$. In a grating with a finite length, the reflection, $\tilde{r}^f(\kappa)$, can be calculated from two simple analytical functions that exist in a finite time region, as described below. The impulse response of the grating can be extracted accurately from the reflection function, defined in the complex frequency plane, by using the inverse Laplace transform instead of the Fourier transform used in previous algorithms.

When the system is unstable, the forward reflection $\tilde{r}^f(\kappa) = \bar{b}(-\kappa)/\bar{a}(-\kappa)$ contains poles in the upper half of the complex plane of κ: $\{\kappa_j\}_{j=1}^N$.[26] Therefore the impulse response can be calculated by using a transformation similar to the inverse Laplace transform:

$$\tilde{h}^f(\tau) = \frac{1}{2\pi}\int_{-\infty+i\mu}^{\infty+i\mu} \tilde{r}^f(\kappa)\exp(-i\kappa\tau)\mathrm{d}\kappa, \qquad (15)$$

where μ is a real constant, chosen in order to perform the integration in a contour that passes above all the singularity points of the reflection function, $\{\kappa_j\}$: $\mu > \max_j(\mathrm{Im}\{\kappa_j\})$.

When the conjugate system is stable, we can choose $\mu = 0$, and Eq. (15) gives the conventional calculation of the impulse response with use of the Fourier transform, as described in Section 2. For calculation of the integral in Eq. (15), the reflection $\tilde{r}(\kappa)$ should be calculated over the contour in the complex plane: $\kappa = k + i\mu$ ($-\infty < k < \infty$). Since the grating length is finite, the solution $\bar{\Psi}(\kappa, z)$ is an analytical function of κ.[24] Using Eqs. (9) and (10), we obtain the boundary condition $\bar{\Psi}(\kappa, z = 0) = (\bar{a}(\kappa), \bar{b}(\kappa))^t$. In Section 2 we showed that the functions $\bar{a}(k)$ and $\bar{b}(k)$ can be calculated from the reflection and transmission functions of the grating $r_m^f(k)$, $r_m^b(k)$, $t_m^f(k)$. Similarly to the derivation in Ref. 24, we express the solution $\bar{\Psi}(\kappa, z)$ by using a kernel vector function $\bar{K}(\tau, z)$:

$$\bar{\Psi}(\kappa, z) = \binom{1}{0}\exp[-i\kappa(z - L)]$$
$$+ \int_{z-L}^{L-z} \bar{K}(\tau, z)\exp(i\kappa\tau)\mathrm{d}\tau, \qquad 0 \leq z \leq L. \qquad (16)$$

The kernel vector function is unequal to zero only in the interval $z - L \leq \tau \leq L - z$. By substituting the solution in Eq. (16) into the coupled-mode equations, Eq. (6), we can show, using the theory of characteristics as performed in Ref. 24, that the kernel functions exist and are unique. Using Eq. (16), we can calculate the time-domain functions $\bar{a}(\tau)$ and $\bar{b}(\tau)$ by performing a Fourier transform on the function $\bar{\Psi}(\kappa, z = 0)$:

$$\binom{\bar{a}(\tau)}{\bar{b}(\tau)} = \binom{\delta(\tau - L)}{0} + \bar{K}(\tau, 0). \qquad (17)$$

Equation (17) shows that the functions $\bar{a}(\tau)$ and $\bar{b}(\tau)$ are unequal to zero only in the interval $-L \leq \tau \leq L$. This result can also be easily obtained by using a discrete model for the grating, which is used in the layer-peeling

algorithm, to be discussed in Section 4. The functions $\bar{a}(\kappa)$ and $\bar{b}(\kappa)$ can be calculated over the contour $\kappa = -(k + i\mu)$ by using

$$\begin{pmatrix} \bar{a}(-k - i\mu) \\ \bar{b}(-k - i\mu) \end{pmatrix} = \begin{pmatrix} \exp[-i(k + i\mu)L] \\ 0 \end{pmatrix}$$
$$+ \int_{-L}^{L} \bar{K}(\tau, 0)\exp[-i(k + i\mu)\tau]\mathrm{d}\tau,$$

(18)

where the kernel function $\bar{K}(\tau, z = 0)$ can be calculated from the boundary conditions by performing a Fourier transform on the functions, $(\bar{a}(k) - \exp(ikL), \bar{b}(k))^t$. The reflection of the conjugate system can now be calculated along the contour $\kappa = k + i\mu$ by using the connection, $\tilde{r}^f(k + i\mu) = \bar{b}(-k - i\mu)/\bar{a}(-k - i\mu)$, and the impulse response of the conjugate system is obtained by using Eq. (15). We note that since the kernel functions $\bar{K}(\tau, 0)$ exist only in a limited time interval, $-L \leq \tau \leq L$, the numerical calculation of Eq. (18) can be easily performed.

The technique for calculating the impulse response described in this section may be also useful when the conjugate system is stable and even in the case when the grating is lossless. When the poles of the reflection function are located in the lower half of the complex plane, close to the real axis of κ, the impulse response decays over a long time interval. In this case the spectral resolution of the reflection function should be high enough to avoid errors due to aliasing effects.[27] On the other hand, the kernel function $\bar{K}(\tau, 0)$ can be easily calculated since it exists only in a limited time interval. By use of the technique described above, the impulse response can be accurately calculated with a smaller frequency resolution than needed when it is calculated directly from the reflection spectrum. Therefore the method described in this section may be helpful even for lossless gratings that have a very high reflectivity.

4. LAYER-PEELING ALGORITHM

In this section we describe the layer-peeling algorithm for extracting the parameters of a grating with loss or gain. The algorithm is based on modeling the grating by using discrete scatterers, as performed for lossless gratings.[16,17] We divide the grating into N layers, each with a width Δz. Each layer is modeled by a discrete reflector, with coupling coefficients q_1 and q_2, and by a free propagation with a length Δz. The layer-peeling algorithm is performed in two steps that are repeated recursively. In the first step, the two coupling coefficients of a layer are extracted from the local forward reflections of the original and the conjugate systems. In the second step, the extracted coupling coefficients are used to propagate the local reflections of the original and the conjugate systems to the next layer. The algorithm is repeated until the entire grating is reconstructed.

In the original system, the fields of layer n are connected to the fields of layer $n + 1$ by the transfer matrix, $T_n(k)$:

$$\begin{pmatrix} u_1(k, (n + 1)\Delta z) \\ u_2(k, (n + 1)\Delta z) \end{pmatrix} = T_n(k)\begin{pmatrix} u_1(k, n\Delta z) \\ u_2(k, n\Delta z) \end{pmatrix}, \quad (19)$$

where

$$T_n = (1 - q_{1,n}q_{2,n}\Delta z^2)^{-1/2}$$
$$\times \begin{bmatrix} \exp(-ik\Delta z) & 0 \\ 0 & \exp(ik\Delta z) \end{bmatrix}\begin{bmatrix} 1 & q_{1,n}\Delta z \\ q_{2,n}\Delta z & 1 \end{bmatrix},$$

(20)

and $q_{i,n} = q_i(z = n\Delta z)$ $(n = 0, 1...N - 1)$.

The matrix in Eq. (20) is an approximation to the transfer matrix used in Refs. 16 and 17. The hyperbolic functions in Ref. 17 were approximated by $\tanh[(q_{1,n}q_{2,n})^{1/2}\Delta z] \simeq (q_{1,n}q_{2,n})^{1/2}\Delta z$. This approximation does not add a significant error, since the assumption that the reflectivity of each grating layer is very low, $(q_{1,n}q_{2,n})^{1/2}\Delta z \ll 1$, is essential for using a discrete model to analyze the grating. The accuracy of this approximation was verified numerically, and we found out that it did not add an observable error to the solution for the examples given in Section 5.

The fields $\tilde{U}(k, z)$ in the conjugate system are propagated through the same equation used in the original problem, Eq. (19); However the transfer matrix for the conjugate system is equal to

$$\tilde{T}_n = (1 - q_{1,n}q_{2,n}\Delta z^2)^{-1/2}\begin{bmatrix} \exp(-ik\Delta z) & 0 \\ 0 & \exp(ik\Delta z) \end{bmatrix}$$
$$\times \begin{bmatrix} 1 & q_{2,n}\Delta z \\ q_{1,n}\Delta z & 1 \end{bmatrix}.$$

We define the local forward reflection for the original and the conjugate problems:

$$r^f(k, z) = u_1(k, z)/u_2(k, z),$$
$$\tilde{r}^f(k, z) = \tilde{u}_1(k, z)/\tilde{u}_2(k, z). \quad (21)$$

The local forward reflections $r^f(k, z)$ and $\tilde{r}^f(k, z)$ are the forward reflections of the grating section located at the region $[z, L]$ for the original and the conjugate system, respectively. The local discrete reflection of each layer of the original and the conjugate system is defined as $r_n^f(k) = r^f(k, n\Delta z)$ and $\tilde{r}_n^f(k) = \tilde{r}^f(k, n\Delta z)$, respectively.

Using Eqs. (19)–(21) we obtain the propagation equations:

$$r_{n+1}^f(k) = \exp(-2ik\Delta z)\frac{r_n^f(k) + q_{1,n}}{1 + r_n^f(k)q_{2,n}}, \quad (22)$$

$$\tilde{r}_{n+1}^f(k) = \exp(-2ik\Delta z)\frac{\tilde{r}_n^f(k) + q_{2,n}}{1 + \tilde{r}_n^f(k)q_{1,n}}. \quad (23)$$

Equations (22) and (23) are a generalization of the equation given in Ref. 17 for lossless gratings.

The forward local impulse response of the original problem, $h_n^f(\tau)$, is obtained by performing a discrete Fourier transform on the local reflection, $r_n^f(k)$.[16,17] The local impulse response, $h_n^f(\tau)$, is equal to the forward impulse response of the grating section located in the grating region $[n\Delta z, L]$. The impulse response at $\tau = 0$ is equal to the average of the reflection function,

$h_n^f(\tau = 0) = 1/M \Sigma_{m=1}^{M} r_n^f(k_m)$, where the sum is taken over all the sampled frequencies of the grating spectrum. Owing to the causality of the system, the local impulse response at $\tau = 0$, $h_n^f(\tau = 0)$ is determined only by the first reflector located at $z = n\Delta z$. The reflection of the single scatterer, which corresponds to the nth layer, is obtained by using Eq. (20), $r_n^f(k) = -q_{1,n}\Delta z$, and therefore the local impulse response at $\tau = 0$ is equal to $h_n^f(\tau = 0) = -q_{1,n}\Delta z$. Thus the coupling coefficient $q_{1,n}$ of each layer can be extracted from the local forward reflection of the original system:

$$q_{1,n} = -\frac{1}{M\Delta z} \sum_{m=1}^{M} r_n^f(k_m). \tag{24}$$

When the conjugate system is stable, the derivation of Eq. (24) can be repeated for the conjugate system. The coupling coefficient $q_{2,n}$ of each layer is extracted from the local forward reflection of the conjugate system:

$$q_{2,n} = -\frac{1}{M\Delta z} \sum_{m=1}^{M} \widetilde{r}_n^f(k_m). \tag{25}$$

When the conjugate system is unstable, or when the duration of the impulse response function of the conjugate system is significantly broader than the minimal duration of the impulse response, $2L$, the method for calculating the forward impulse response of the conjugate system described in Section 3 can be used. The use of the new method will permit the reduction of the bandwidth that is needed to sample the reflection spectrum. The first step in calculating the impulse-response function is to calculate the reflection over a contour in the complex plane, $\widetilde{r}^f(k + i\mu)$, as described in Section 3. The forward reflection function of the conjugate system is then propagated by using

$$\widetilde{r}_{n+1}^f(k + i\mu) = \exp(-2i(k + i\mu)\Delta z)\frac{\widetilde{r}_n^f(k + i\mu) + q_{2,n}}{1 + \widetilde{r}_n^f(k + i\mu)q_{1,n}} \tag{26}$$

instead of Eq. (22). The extraction of the coupling coefficient $q_2(z)$ is performed by using

$$q_{2,n} = -\frac{1}{M\Delta z} \sum_{m=1}^{M} \widetilde{r}^f(k_m + i\mu) \tag{27}$$

instead of Eq. (24).

The layer-peeling algorithm may now be summarized:

1.   Obtain $r_0^f(k)$ and calculate the reflection of the conjugate system $\widetilde{r}_0^f(k)$ or $\widetilde{r}_0^f(k + i\mu)$ from the input data.
2.   Use Eqs. (24) and (25) or Eqs. (24) and (27) to find the coupling coefficients of the current layer.
3.   Use Eqs. (22) and (23) or Eqs. (22) and (26) to propagate the reflections to the next layer.
4.   Repeat steps 2 and 3 until the entire grating structure is reconstructed.

5.   NUMERICAL RESULTS

We demonstrate in this section the implementation of our layer-peeling algorithm for reconstructing the profiles of three lossy gratings. The gratings that were reconstructed had either a stable or an unstable conjugate system. Accurate reconstruction was obtained for all three examples given in this section. The transmission and the reflection from both sides of the grating were calculated numerically by dividing the gratings into 201 small sections and multiplying the transfer matrices of all the sections.[22,23]

In the first example, we studied a grating with a chirped Gaussian profile, written in the region $[0, \mathrm{L} = 1\ \mathrm{cm}]$. The coupling coefficient of the grating is given by $q(z) = 600 \exp[-10^5(z - L/2)^2(2.5 + 20i)]\ \mathrm{m}^{-1}$. The loss coefficient is sinusoidal and is equal to $\alpha(z) = 70[1 - \cos(10\pi z/L)]\ \mathrm{m}^{-1}$. The maximum reflectivity and transmissivity of the grating are equal to 0.11 and 0.246, respectively. The reflection from both sides of the grating and the transmission functions were sampled over a bandwidth of 10 nm with a spectral resolution of 0.02 nm. Figure 1 shows the profile of the reconstructed amplitude $|q(z)|$, the phase of the coupling coefficient $\arg[q(z)]$, and the profile of the loss coefficient $\alpha(z)$. The figure compares the reconstructed grating parameters (solid curves) and the original parameters (dashed curves). The figure demonstrates that all three grating parameters were accurately reconstructed.

In the second example, we reconstructed a grating written in the region $[0, \mathrm{L} = 20\ \mathrm{mm}]$, with a uniform coupling coefficient $q(z)$ and a Gaussian loss profile. The amplitude of the coupling coefficient of the grating is equal to $|q| = 30\ \mathrm{m}^{-1}$. The phase derivative of the coupling coefficient is given by $\mathrm{d}/\mathrm{d}z[\arg(q)] = 120 \exp[-(z - L/2)^2/1.6 \times 10^{-5}]\ \mathrm{m}^{-1}$. The phase derivative of the coupling coef-
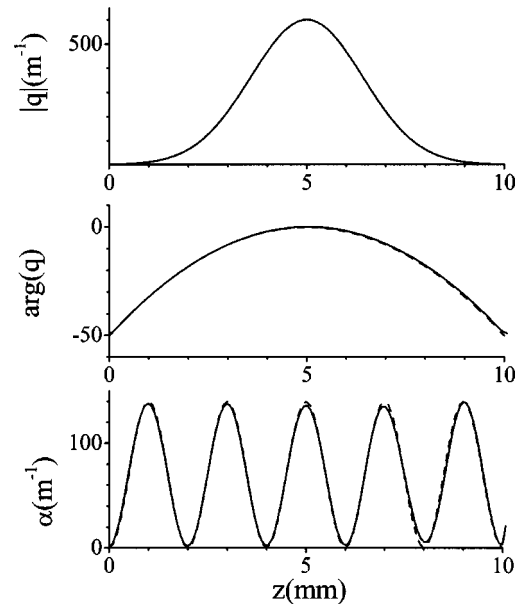
Fig. 1.   Reconstruction of a grating with a chirped Gaussian coupling coefficient, $q(z) = 600 \exp[-10^5(z - L/2)^2(2.5 + 20i)]\ \mathrm{m}^{-1}$ and with a sinusoidal loss profile $\alpha = 70[1 - \cos(10\pi z/L)]\ \mathrm{m}^{-1}$ written in the region $[0, \mathrm{L} = 1\ \mathrm{cm}]$. The reconstructed parameters (solid curves) are compared with the original parameters (dashed curves). The reflection spectra, obtained from both sides of the grating, and the transmission spectrum were sampled over a bandwidth of 10 nm with a spectral resolution of 0.02 nm.
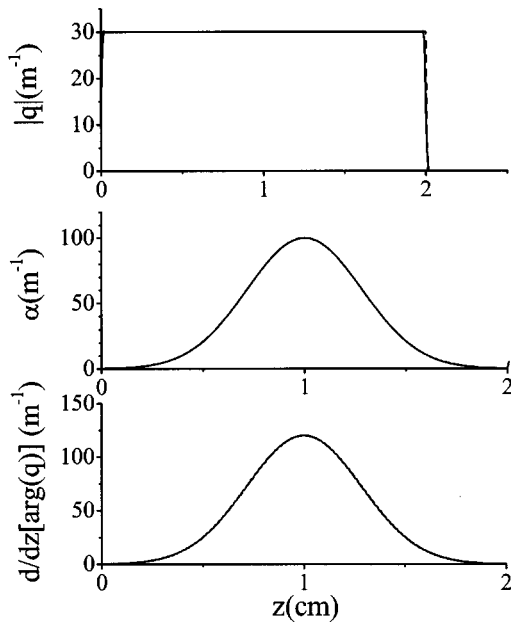
Fig. 2.   Reconstruction of a grating with a coupling coefficient, $|q| = 30 \, \mathrm{m}^{-1}$, a Gaussian phase derivative, $\mathrm{d}/\mathrm{d}z[\arg(q)] = 120 \exp[-(z - L/2)^2/1.6 \times 10^{-5}] \, \mathrm{m}^{-1}$, and a Gaussian loss coefficient $\alpha(z) = 100 \exp[-(z - L/2)^2/1.6 \times 10^{-5}] \, \mathrm{m}^{-1}$, written in the region $[0, L = 2 \, \mathrm{cm}]$. The reconstructed parameters (solid curves) are compared with the original parameters (dashed curves). The reflection spectra, obtained from both sides of the grating, and the transmission spectrum were sampled over a bandwidth of 10 nm with a spectral resolution of 0.005 nm.

ficient is proportional to the change in the average refractive index of the grating [Eq. (8)]. In a fiber Bragg sensor, the change in the average refractive index is connected to variations in the environmental conditions such as temperature or strain.[12] The loss coefficient is equal to $\alpha(z) = 100 \exp[-(z - L/2)^2/1.6 \times 10^{-5}] \, \mathrm{m}^{-1}$, and the maximum reflectivity and transitivity of the grating are 0.11 and 0.242, respectively. The reflection from both sides of the grating and the transmission were sampled over a bandwidth of 10 nm with a spectral resolution of 0.005 nm. To reduce the ripples in the impulse-response function, we used a Hanning window to calculate the impulse response from its Fourier transform. The ripples are caused by the abrupt change at the boundaries of the grating. We note that although the Hanning window may add a small error in the reconstruction of the index profile of the grating,[18] it reduces significantly the error in extracting the loss coefficient $\alpha(z)$. The loss coefficient is calculated from the coupling coefficients $q_1(z)$ and $q_2(z)$ by using a derivative operation [Eqs. (7)]. Therefore the extraction of the loss coefficient $\alpha(z)$ may become sensitive to ripples in the extracted coupling coefficients. The amplitude and the phase derivative of the coupling coefficient $q(z)$ and the loss coefficient $\alpha(z)$ are shown in Fig. 2. A comparison between the reconstructed grating parameters (solid curves) and the original parameters (dashed curves) shows that an excellent reconstruction was obtained.

In the third example we reconstruct a grating with an unstable conjugate system. The coupling coefficient of the grating is equal to $q(z) = 250[1 + 0.9 \cos(2\pi z/L)] \, \mathrm{m}^{-1}$, and the loss coefficient is given by

$\alpha(z) = 250[1 - \cos(2\pi z/L)] \, \mathrm{m}^{-1}$. The length of the grating is equal to $L = 4 \, \mathrm{mm}$. The maximum reflectivity and transmissivity of the grating are 0.23 and 0.135, respectively. The reflection from both sides of the grating and the transmission functions were sampled over a bandwidth of 20 nm with a spectral resolution of 0.01 nm. A Hanning window was used to reduce the ripples in the impulse-response functions that were due to the sharp jump at the grating boundaries. Figure 3(a) shows the Fourier transform of the forward reflection function of the conjugate system. The figure clearly shows that the calculated Fourier transform is a noncausal function and therefore does not equal the impulse-response function of the grating which should be a causal function. The impulse response, shown in Fig. 3(b), was calculated with the method described in Section 3. The calculation of the impulse response was performed by using Eq. (15) on a contour $\kappa = k + i\mu$, where $\mu = 100 \, \mathrm{m}^{-1}$. The integration contour was chosen above all the singularity points of the reflection function. The location of the dominant pole in the reflection spectrum was estimated from the noncausal function calculated by performing the Fourier transform on the forward reflection spectrum of the conjugate system. The Fourier transform of the forward reflection spectrum of the conjugate system, $\tilde{r}^f(k)$, is given by[26]

$$f(\tau) = \frac{1}{2\pi} \int_{-\infty}^{\infty} \tilde{r}^f(k) \exp(-ik\tau) \mathrm{d}k$$

$$= \sum_{j=1}^{N} c_j \exp(-i\kappa_j \tau) \quad \text{for} \quad \tau < 0, \qquad (28)$$

where $\{\kappa_j\}$ are the poles of the forward reflection spectrum. We used an exponential fit to estimate the growth rate of the noncausal function $f(\tau)$ at a negative time, $\tau < 0$. We chose the contour constant μ to be larger than the estimated growth rate.
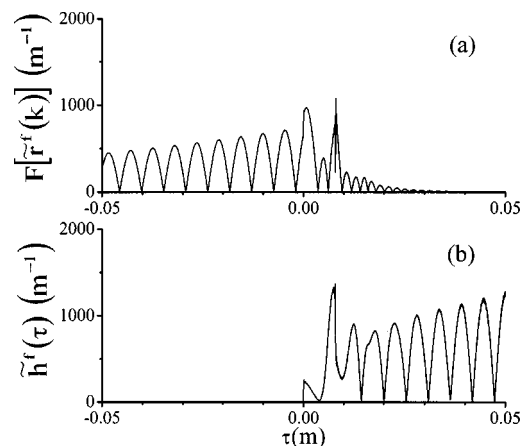
Fig. 3.   (a) Fourier transform of the forward reflection function of an unstable conjugate system and (b) the forward impulse response, calculated with the method described in Section 3. The coupling-coefficient profile of the grating was equal to $q(z) = 250[1 + 0.9 \cos(2\pi z/L)] \, \mathrm{m}^{-1}$, and the loss profile was given by $\alpha(z) = 250[1 - \cos(2\pi z/L)] \, \mathrm{m}^{-1}$. The grating was written in the region $[0, L = 4 \, \mathrm{mm}]$. The Fourier transform of the grating reflection spectrum gives a wrong result since it corresponds to a noncausal function.
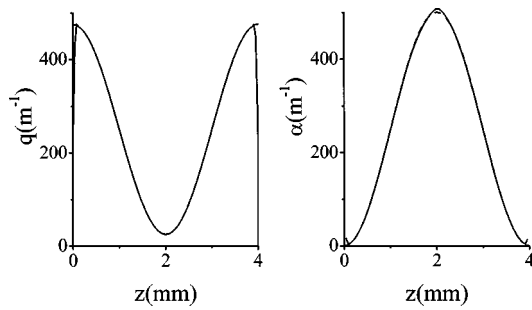
Fig. 4.   Reconstruction of a grating with an unstable conjugate system, analyzed in Fig. 3.   The grating was written in the region $[0, L = 4 \text{ mm}]$ and had a coupling-coefficient profile of $q(z) = 250[1 + 0.9 \cos(2\pi z/L)] \, \text{m}^{-1}$ and a loss profile $\alpha(z) = 250[1 - \cos(2\pi z/L)] \, \text{m}^{-1}$.   Since the conjugate system is unstable, the impulse-response function was calculated with the method described in Section 3.   The reconstructed parameters (solid curves) are compared with the original parameters (dashed curves).

The reconstructed grating parameters are shown in Fig. 4.   The figure shows that the reconstructed parameters (solid curves) are in excellent agreement with the original parameters (dashed curves).   The small error in the extracted loss coefficient at the boundaries of the grating is due to the sharp change in the coupling coefficient at the grating boundaries.

6. CONCLUSIONS

We have demonstrated an inverse scattering algorithm for reconstructing lossy fiber Bragg gratings.   The algorithm permits extraction of the profiles of the refractive index and the loss coefficient along the grating from the grating transmission spectrum and the reflection spectra, measured from both sides of the grating.   A new method to overcome instability problems that may occur in reconstructing fiber Bragg gratings was demonstrated.   The method may also permit reduction of the spectral resolution needed to reconstruct highly reflecting fiber Bragg gratings without loss.   The algorithm for reconstructing the structure of a lossy grating was demonstrated numerically, and it gave excellent results for both stable and unstable conjugate systems.   The algorithm demonstrated in this paper may be used to develop new types of evanescent-field fiber Bragg sensors that make it possible to detect the spatial distribution of both the absorption and the refractive index along the grating.   The algorithm can also be used to analyze fiber Bragg gratings written in fiber amplifiers and in fiber lasers.

ACKNOWLEDGMENTS

The authors may be reached by email as follows: Amir Rosenthal, eeamir@tx.technion.ac.il;   Moshe Horowitz, horowitz@ee.technion.ac.il.

REFERENCES

1.   A. D. Kersey, "A Review of recent developments in fiber optic sensors technology," Opt. Fiber Technol. **2**, 291–317 (1996).
2.   V. Goloborodko, S. Keren, A. Rosenthal, B. Levit, and M. Horowitz, "Measuring temperature profiles in high-power optical components," Appl. Opt. **42**, 2284–2288 (2003).
3.   S. Huang, M. M. Ohn, M. LeBlanc, and R. M. Measures, "Continuous arbitrary strain profile measurements with fiber Bragg gratings," Smart Mater. Struct. **7**, 248–256 (1998).
4.   M. Volanthen, H. Geiger, M. J. Cole, and J. P. Dakin, "Measurement of arbitrary strain profiles within fibre gratings," Electron. Lett. **32**, 1028–1029 (1996).
5.   P. H. Paul and G. Kychakoff, "Fiber-optic evanescent field absorption sensor," Appl. Phys. Lett. **51**, 12–14 (1987).
6.   H. Tai, H. Tanaka, and T. Yoshino, "Fiber-optic evanescent-wave methane-gas sensor using optical absorption for the 3.392-μm line of a He–Ne laser," Opt. Lett. **12**, 437–439 (1987).
7.   V. Ruddy, B. D. MacCraith, and J. A. Murphy, "Evanescent wave absorption spectroscopy using multimode fibers," J. Appl. Phys. **67**, 6070–6074 (1990).
8.   G. P. Anderson, J. P. Golden, L. K. Cao, D. Wijesuriya, L. C. Shriver-Lake, and F. S. Ligler, "Development of an evanescent wave fiber optic biosensor," IEEE Eng. Med. Biol. Mag. **13**, 358–363 (1994).
9.   A. Messica, A. Greenstein, and A. Katzir, "Theory of fiber-optic, evanescent-wave spectroscopy and sensors," Appl. Opt. **35**, 2274–2284 (1996).
10.   S. K. Khijwania and B. D. Gupta, "Fiber optic evanscent field absorption sensor: effect of fiber parameters and geometry of the probe," Opt. Quantum Electron. **31**, 625–636 (1999).
11.   P. K. Choudhury and T. Yoshino, "On the optical sensing means for the study of chemical kinetics," Meas. Sci. Technol. **13**, 1793–1797 (2002).
12.   K. Schroeder, W. Ecke, R. Mueller, R. Willsch, and A. Andreev, "A fibre Bragg grating refractometer," Meas. Sci. Technol. **12**, 757–764 (2001).
13.   J. Dubendorfer, R. E. Kunz, G. Jobst, I. Moser, and G. Urban, "Integrated optical pH sensor using replicated chirped grating coupler sensor chips," Sens. Actuators B **50**, 210–219 (1998).
14.   S. Keren and M. Horowitz, "Distributed three-dimensional fiber Bragg grating refractometer for biochemical sensing," Opt. Lett. **28**, 2037–2039 (2003).
15.   S. Keren and M. Horowitz, "Interrogation of fiber gratings by use of low-coherence spectral interferometry of noiselike pulses," Opt. Lett. **26**, 328–330 (2001).
16.   R. Feced, M. N. Zervas, and M. A. Muriel, "An efficient inverse scattering algorithm for the design of nonuniform fiber Bragg gratings," IEEE J. Quantum Electron. **35**, 1105–1115 (1999).
17.   J. Skaar, L. Wang, and T. Erdogan, "On the synthesis of fiber Bragg gratings by layer peeling," J. Lightwave Technol. **37**, 165–173 (2001).
18.   A. Rosenthal and M. Horowitz, "Inverse scattering algorithm for reconstructing strongly reflecting fiber Bragg gratings," IEEE J. Quantum Electron. **39**, 1018–1026 (2003).
19.   A. M. Bruckstein, B. C. Levy, and T. Kailath, "Differential methods in inverse scattering," SIAM (Soc. Ind. Appl. Math.) J. Appl. Math. **45**, 312–335 (1985).
20.   J. Frolik and A. E. Yagle, "Forward and inverse scattering for discrete layered lossy and absorbing media," IEEE Trans. Circuits Syst. **44**, 710–722 (1997).
21.   W. H. Loh and R. I. Laming, "1.55 μm phase-shifted distributed feedback fibre laser," Electron. Lett. **31**, 1440–1442 (1995).

22. H. Kogelnik, "Coupled wave theory for thick hologram gratings," Bell Syst. Tech. J. **48**, 2909–2947 (1969).
23. T. Erdogan, "Fiber grating spectra," J. Lightwave Technol. **15**, 1277–1294 (1997).
24. M. J. Ablowitz and H. Segur, *Solitons and the Inverse Scattering Transform* (Society for Applied Mathematics, Philadelphia, Pa., 1981).
25. S. Keren, A. Rosenthal, and M. Horowitz, "Measuring the structure of highly reflecting fiber Bragg gratings," IEEE Photon. Technol. Lett. **15**, 575–577 (2003).
26. A. Papoulis, *The Fourier Integral and Its Applications* (McGraw-Hill, New York, 1962).
27. J. G. Proakis and D. G. Manolakis, *Digital Signal Processing: Principles, Algorithms, and Applications*, 3rd ed. (Prentice-Hall International, London, 1996).